Journal of Materials Chemistry B

ROYAL SOCIETY OF CHEMISTRY

PAPER

View Article Online
View Journal | View Issue

Cite this: *J. Mater. Chem. B*, 2023, **11**, 8422

Single stop analysis of a protein surface using molecular probe electrochemistry†

Jewel Ann Maria Xavier, Isabel Fuentes, Miquel Nuez-Martínez, Clara Viñas and Francesc Teixidor *

Visualization of a protein in its native form and environment without any interference has always been a challenging task. Contrary to the assumption that protein surfaces are smooth, they are in fact highly irregular with undulating surfaces. Hence, in this study, we have tackled this ambiguous nature of the 'surface' of a protein by considering the 'effective' protein surface (EPS) with respect to its interaction with the geometrically well-defined and structurally inert anionic molecule $[3,3'\text{-Co}(1,2\text{-}C_2B_9H_{11})_2]^-$, abbreviated as [*o*-COSAN]$^-$, whose stability, propensity for amine residues, and self-assembling abilities are well reported. This study demonstrates the intricacies of protein surfaces exploiting simple electrochemical measurements using a 'small molecule' redox-active probe. This technique offers the advantage of not utilizing any harsh experimental conditions that could alter the native structure of the protein and hence the protein integrity is retained. Identification of the amino acid residues which are most involved in the interactions with $[3,3'\text{-Co}(1,2\text{-}C_2B_9H_{11})_2]^-$ and how a protein's environment affects these interactions can help in gaining insights into how to modify proteins to optimize their interactions particularly in the fields of drug design and biotechnology. In this research, we have demonstrated that $[3,3'\text{-Co}(1,2\text{-}C_2B_9H_{11})_2]^-$ anionic small molecules are excellent candidates for studying and visualizing protein surfaces in their natural environment and allow proteins to be classified according to the surface composition, which imparts their properties. $[3,3'\text{-Co}(1,2\text{-}C_2B_9H_{11})_2]^-$ 'viewed' each protein surface differently and hence has the potential to act as a simple and easy to handle cantilever for measuring and picturing protein surfaces.

Received 12th April 2023,
Accepted 28th July 2023

DOI: 10.1039/d3tb00816a

rsc.li/materials-b

Introduction

The shape of a protein is a consequence of the order of its amino acids, its hydrogen bond interactions, and very fundamentally its tertiary structure, which is influenced by the environment in which the protein operates. All of these factors define a protein's function, since the protein's ability to interact with other molecules depends on its structure, and a fundamental aspect of this interaction is the protein's surface.[1,2] The 'surface' of a protein is an ambiguous term as it depends on a number of factors, most notably the specific environment in which the protein is situated. The effect of different ions and solvent molecules surrounding the protein on its structure is significant. Most often, a ball-park surface area is calculated by considering the hydrodynamic or Stokes radius in the case of proteins. In this approximation, a uniform sphere with a smooth surface having the same hydrodynamic properties as the biomolecule is considered.[3,4] A major drawback to this approximation is that it does not account for the protein shape, which can be either globular or non-globular and is highly irregular, nor the environment of the protein.[5–8] The interaction of the amino acid residues with different ions can result in altering the surface of the proteins.[9–11] Contrary to the assumption that protein surfaces are smooth, they are in fact highly irregular with undulating surfaces. The current state-of-the-art techniques for studying a protein are either by X-ray and neutron diffraction studies of crystallized proteins, cryo-electron microscopy (cryo-EM), and nuclear magnetic resonance (NMR) spectroscopy or through computer modelling.[12–20] Recent developments in the field of fluorescence imaging have shown the use of dyes forming covalent bonds with specific amino acid residues such as lysine-161 in human serum albumin (HSA) for *in-vivo* studies which also allows for better understanding of the proteins.[21,22] Studies involving direct electrochemical measurements of proteins to assess the surface are common but more often tend to subject the proteins to unnecessary stresses such as application of high voltage leading to denaturalization.[23–25] Moreover, most of the

Institut de Ciencia de Materials de Barcelona (ICMAB-CSIC), Campus de la UAB, Bellaterra, Spain. E-mail: jxavier@icmab.es, isa7391@gmail.com, mnuez@icmab.es, clara@icmab.es, teixidor@icmab.es

† Electronic supplementary information (ESI) available. See DOI: https://doi.org/10.1039/d3tb00816a

redox active amino acids such as tyrosine and tryptophan are non-polar and hence prefer to be located in the interior of the proteins with very few residues on the surface.[26] All these strategies fail to visualize the protein in its native form and environment. Therefore, to overcome this problem, we reasoned, why not reap the benefits from an electroactive compound external to the protein that interacts strongly with the polar residues and has self-assembling properties? The approach is challenging as we would need a water-soluble substance which is redox-reversible, has an electrochemical response well within the window of application in water, interacts rapidly and strongly with the basic groups on the residues and has self-assembly properties so as to fill the available surface area of the protein to the maximum extent. What could be the substance that satisfies all these requirements?

In this study, we aim at gaining molecular level understanding of the 'effective protein surface' (EPS) using a geometrically well-defined and structurally inert anionic molecule $[3,3'\text{-Co}(1,2\text{-}C_2B_9H_{11})_2]^-$, known as $[o\text{-COSAN}]^-$, whose stability, tendency for amine residues through the formation of strong N–H···B–H di hydrogen bonds and self-assembling abilities are well documented.[27–32] Another notable type of assembly that has been reported is based on the *nido*-$[C_2B_9H_{11}]^-\cdots\pi$ interactions. These interactions give rise to a range of photophysical properties, including aggregation-induced emission and aggregation-caused quenching, all within a single molecule.[33] The 'effective protein surface' describes the actual protein form with its anomalies and irregularities in its native environment contrary to the smooth sphere visualized using the Stokes radius. $[3,3'\text{-Co}(1,2\text{-}C_2B_9H_{11})_2]^-$ is a θ-shaped metallacarborane complex where the metal ion is sandwiched between the two dicarbollide clusters. Depending on the relative positions of the carbon atoms, three distinct rotamers can be observed (Fig. 1a), Previously, we had observed and demonstrated using DFT calculations that the cisoid rotamer exhibits a distinct 'hydrophilic' polar head region and a 'hydrophobic' apolar tail region.[28] This unique configuration enables the cisoid rotamer to display surfactant-like behavior, contrary to the transoid rotamer (Fig. 1b).[34] Moreover, the reversible redox capacity of $[3,3'\text{-Co}(1,2\text{-}C_2B_9H_{11})_2]^-$ and $[3,3'\text{-Fe}(1,2\text{-}C_2B_9H_{11})_2]^-$ in water has also been well defined and these molecules have been postulated as universal internal ref. 35. Thus, using readily available electrochemical cyclic voltammetry or differential pulse electrochemical techniques and $[3,3'\text{-Co}(1,2\text{-}C_2B_9H_{11})_2]^-$, we will learn about the EPS and establish the mechanisms of ion–protein interactions. We propose $[3,3'\text{-Co}(1,2\text{-}C_2B_9H_{11})_2]^-$ as a 'small molecule probe' analogous to a cantilever in scanning transmission electron microscopy (STEM) for identifying the nature of a protein's surface in its native or almost native form.[36,37]

We, among others, have recently demonstrated that the $[3,3'\text{-Co}(1,2\text{-}C_2B_9H_{11})_2]^-$ anion strongly interacts with bovine serum albumin (BSA) with a molar ratio 100 : 1.[38–40] The interaction as well as the molar ratio were assessed by measuring the changes in physical properties, including fluorescence and size, through techniques such as fluorescence spectroscopy, dynamic light scattering (DLS), zeta potential analysis, or studying the precipitated complex using energy-dispersive X-ray spectroscopy (EDX) or elemental analysis. Among these studies, dynamic light scattering (DLS) and zeta potential measurements played a crucial role. DLS provided valuable information about the hydrodynamic diameter of the complex, allowing us to propose a model in which BSA is encapsulated by $[3,3'\text{-Co}(1,2\text{-}C_2B_9H_{11})_2]^-$ in an end-on position. On the other hand, zeta potential measurements reaffirmed the presence of the anion on the BSA surface by confirming the negative charge it imparted. Interestingly, the total number of basic amino acid (lysine, arginine and histidine) residues in a BSA molecule is also 100 which coincides with the number of $[3,3'\text{-Co}(1,2\text{-}C_2B_9H_{11})_2]^-$.[41,42] If we were to consider that $[3,3'\text{-Co}(1,2\text{-}C_2B_9H_{11})_2]^-$ interacts strongly with the basic amino acid residues, the conclusion seemed very straightforward. There was one $[3,3'\text{-Co}(1,2\text{-}C_2B_9H_{11})_2]^-$ for every basic residue. Would it all be that easy? Or is the BSA an ideal model? We will see throughout this article that there are several other factors that must influence the ratio of $[3,3'\text{-Co}(1,2\text{-}C_2B_9H_{11})_2]^-$ molecules *vs.* basic residues. We have postulated the potential application of $[3,3'\text{-Co}(1,2\text{-}C_2B_9H_{11})_2]^-$ as a 'universal' robust shield on proteins which would protect them from denaturalization at high temperatures and retain their activity, irrespective of the nature of the protein.[38] But it was not to be, as the initial experiments with enzymes suggested that $[3,3'\text{-Co}(1,2\text{-}C_2B_9H_{11})_2]^-$

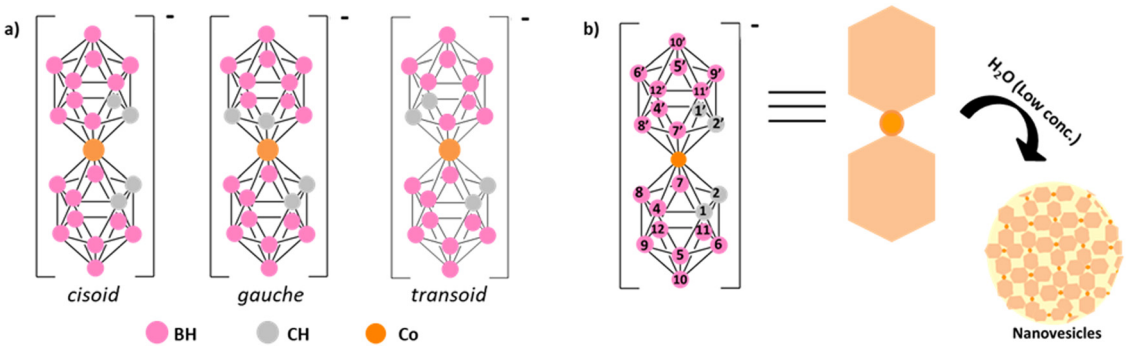

Fig. 1 (a) Schematic representation of the three different rotamers of $[o\text{-COSAN}]^-$: cisoid, *gauche* and transoid. (b) The formation of nanovesicles at a low concentration of the *cis*-$[o\text{-COSAN}]^-$ rotamer in an aqueous solvent.

was not capable of shielding them all. This beseeched us to ponder on whether $[3,3'\text{-Co}(1,2\text{-}C_2B_9H_{11})_2]^-$ really viewed all protein surfaces in the same way.

Interestingly, the strong interaction between the BSA and the $[3,3'\text{-Co}(1,2\text{-}C_2B_9H_{11})_2]^-$ cage raises high expectations such as that suggested by Goszczynski and coworkers to enhance the activity of therapeutic peptides.[43] Our primary investigations were carried out with BSA and $[3,3'\text{-Co}(1,2\text{-}C_2B_9H_{11})_2]^-$ in pure water, without any buffer or other additives.[38,44] In the body, however, the proteins are in an environment with a high electrolyte content and physiological pH. Hence, it is rationale to investigate the behavior of θ-metallacarboranes under physiological conditions and to draw conclusions about the capabilities of $[3,3'\text{-Co}(1,2\text{-}C_2B_9H_{11})_2]^-$ in understanding the protein surface better. In this article, we address these issues and provide a method for interpreting the protein surface areas in terms of EPS. Hence, the study developed here focuses on the application of simple electrochemical techniques for understanding the EPS and consequently its properties and functions under native or near native conditions using a highly suitable redox reversible probe.[45]

The electrochemical experiments are performed in 0.1 M NaCl which acts as the electrolyte. Both Na^+ and Cl^- are part of the Hofmeister series and are chaotropic in nature.[46,47] As a result, the hydrodynamic radius varies in the presence and absence of NaCl and hence the surface area. We also hypothesize that in the presence of NaCl, the polar amino acid residues become even more exposed in comparison to pure water which could imply an even higher ratio of $[3,3'\text{-Co}(1,2\text{-}C_2B_9H_{11})_2]^-$ on the surface, limited by surface availability due to the plausible competition between $[3,3'\text{-Co}(1,2\text{-}C_2B_9H_{11})_2]^-$ and the anions in the electrolyte. The cyclic voltammetry method adopted is gentle enough to avoid protein denaturation, especially considering the protective effect of $[3,3'\text{-Co}(1,2\text{-}C_2B_9H_{11})_2]^-$. In this work, we successfully demonstrate the feasibility of $[3,3'\text{-Co}(1,2\text{-}C_2B_9H_{11})_2]^-$ as a 'small molecule' probe interacting with protein residues within their natural environment. Moreover, our findings reveal that the graphical profile of current intensity *versus* protein concentration differs across the proteins investigated. Although these comparisons have been conducted experimentally, we are certain that with the aid of an appropriate algorithm, we could obtain high-resolution visualizations of the protein surface within its natural environment.

Results and discussion

Experimental evidence for the interaction of $[o\text{-COSAN}]^-$ with basic amino acids

The preparation of the electroactive component in potentiometric membranes for the detection of amino acids was based on the high insolubility of the [YH] $[3,3'\text{-Co}(1,2\text{-}C_2B_9H_{11})_2]$ salt in water, with Y being the amino acid under consideration.[42,48] The same concept was applied to stabilize magnetic nanoparticles decorated with amine groups incorporating $[3,3'\text{-Co}(1,2\text{-}C_2B_9H_{11})_2]^-$ anions.[49] However, these studies offered a vague and general overview of the possible interactions. Hence, in order to gain a deeper insight particularly at the molecular level, a study was performed to visualize the $[3,3'\text{-Co}(1,2\text{-}C_2B_9H_{11})_2]^-$/amino acid interaction *via* ^{1}H- and ^{11}B-NMR spectroscopies to observe the variations in the resonances assumed to be involved in the $[3,3'\text{-Co}(1,2\text{-}C_2B_9H_{11})_2]^-$/amino acid interaction [refer the ESI† for further details].

The experiments were performed at a fixed Na$[3,3'\text{-Co}(1,2\text{-}C_2B_9H_{11})_2]$ concentration of 2 mM in D_2O with increasing concentrations of the amino acids. The influence of the amino acid on the whole spectrum was studied and the resonance due to the B–H of $[3,3'\text{-Co}(1,2\text{-}C_2B_9H_{11})_2]^-$ appearing at 2.60 ppm was taken as the reference (Fig. S1, ESI†). The amino acids studied were L-glutamine, L-arginine, L-lysine and L-histidine of which the latter three contain basic functionalities in the side chains, while L-glutamine was chosen as a representative amino acid for other amino acids such as serine, methionine or alanine, among many others.

Fig. 2 encompasses the results of this study and it can be observed that for the basic amino acids, L-arginine, L-lysine and L-histidine, the intensity of the ^{1}H{^{11}B}-NMR $[3,3'\text{-Co}(1,2\text{-}C_2B_9H_{11})_2]^-$ B–H (4,4′,7,7′) signal decreases as a consequence of the increase of the amino acid/$[3,3'\text{-Co}(1,2\text{-}C_2B_9H_{11})_2]^-$ ratio (Fig. S3, S5 and S7, ESI†). However, this decrement is neither proportional to the amount of the amino acid added which seems to indicate the existence of an equilibrium, nor is it equal for all the three amino acids studied. For instance, in the case of lysine, the B–H signal in the ^{1}H-{^{11}B} NMR vanishes completely, while the decrease in intensity is

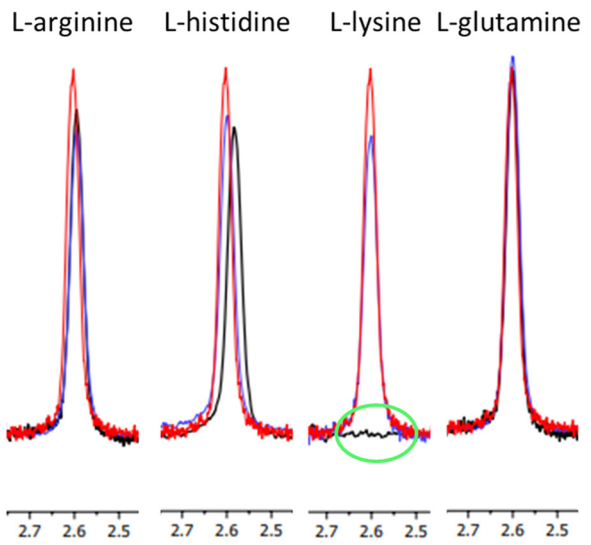

Fig. 2 ^{1}H{^{11}B}-NMR spectra in the range of 2.8 to 2.4 ppm B–H (4,4′,7,7′) obtained for the different mixtures of $[o\text{-COSAN}]^-$ and the amino acids (L-arginie, L-histidine, L-lysine and L-glutamine). Na[*o*-COSAN] 2 mM appears in red, Na[*o*-COSAN] 2 mM + 2 mM of the corresponding amino acid appears in blue and Na[*o*-COSAN] 2 mM + 60 mM of the corresponding amino acid appears in black; the green circle highlights the flatline due to interaction with L-lysine at 60 mM. The solvent used was D_2O.

limited in the case of arginine and histidine and such a decrease was not observed for glutamine (Fig. 2).

These data already suggest that the interaction of different amino acids with $[3,3'\text{-Co}(1,2\text{-}C_2B_9H_{11})_2]^-$ is not the same; strong for the amino acids with basic residues with L-lysine having the strongest interaction and weak or non-existent for the remaining amino acids. And what can be the origin for the disappearance of the B–H resonances? Our interpretation is that nanoscopic aggregates are generated between the basic amino acids and $[3,3'\text{-Co}(1,2\text{-}C_2B_9H_{11})_2]^-$, which are much larger than the individual components and are likely to take on a landscape layout. When $[3,3'\text{-Co}(1,2\text{-}C_2B_9H_{11})_2]^-$ molecules form aggregates with basic amino acids, the local environment around each molecule changes. This altered environment affects the electronic properties and motion of the molecules, leading to changes in the NMR signal. The formation of aggregates can cause significant line broadening, making the signal appear wider and less distinct in the NMR spectrum.[34] It should be noted that neither colloids nor precipitates were observed during the measurement of these experiments.

Consistent with these results are the $^{11}B\{^1H\}$-NMR spectra of the $[3,3'\text{-Co}(1,2\text{-}C_2B_9H_{11})_2]^-$/amino acid complexes. The $^{11}B\{^1H\}$-NMR spectrum of $Na[3,3'\text{-Co}(1,2\text{-}C_2B_9H_{11})_2]$ displays different characteristics when recorded in water or in acetone (Fig. S2, ESI†). In water, the different signals are much wider than in acetone because in one case, the spectra recorded correspond to free rotating molecules, whereas in water, the spectrum of aggregates is recorded, due to self-assembly, forming larger structures that are more difficult to rotate. Therefore, the $^{11}B\{^1H\}$-NMR spectrum will be broader when there is interaction between $[3,3'\text{-Co}(1,2\text{-}C_2B_9H_{11})_2]^-$ and the amino acid. And in fact, that is what has been observed (Fig. S4 and S6, ESI†). Although there is a decrease in the intensity of the signal, it does not disappear as in the case of the proton spectrum; instead it widens, but not to the point of fading. As observed in the case of $^1H\{^{11}B\}$-NMR, the interaction is more evident with L-lysine than for L-arginine and L-histidine, and no signal affectation is observed with glutamine (Fig. 3).

Intensity of current *vs.* ratio of [protein]/[*o*-COSAN]$^-$

The study involves dissolving a given amount of the electrochemically redox-reversible $Na[Co(C_2B_9H_{11})_2]$ to which increasing amounts of a protein are added and the current is measured in response to varying potential levels [refer the ESI† for further details]. To perform the experiment, both $[3,3'\text{-Co}(1,2\text{-}C_2B_9H_{11})_2]^-$ and the protein must be soluble in water. Since an amperometric property is to be measured, an electrolyte is required, which allows the protein to be in an environment comparable to the physiological one. A point to be pondered upon is that neither the applied potential nor the current intensity conditions should affect the stability of the protein. Following this experiment, a graph is obtained from the DPV (differential pulse voltammetry) experiment, wherein the concentration of $[3,3'\text{-Co}(1,2\text{-}C_2B_9H_{11})_2]^-$ remains constant, while the protein concentration increases sequentially (Fig. S9, ESI†). A similar experiment has also been described using $[3,3'\text{-Fe}(1,2\text{-}C_2B_9H_{11})_2]^-$ and its interaction with DNA for developing a DNA bio-sensor.[50] The major contribution to the intensity (current, μA) is from $[3,3'\text{-Co}(1,2\text{-}C_2B_9H_{11})_2]^-$ that remains free in the solution. Although $[3,3'\text{-Co}(1,2\text{-}C_2B_9H_{11})_2]^-$ bound to the protein can also participate in the electron transfer process involving the electrode, the intensity would be much lower in comparison to free $[3,3'\text{-Co}(1,2\text{-}C_2B_9H_{11})_2]^-$ and hence for initial purposes, it can be considered negligible. Thus, the current is the highest in the absence of any interacting protein and decreases with the increasing amount of protein in the solution, but it never intersects the y-axis at 0 because of the bounded $[3,3'\text{-Co}(1,2\text{-}C_2B_9H_{11})_2]^-$. As mentioned before, we are not considering the residual intensity due to the bounded $[3,3'\text{-Co}(1,2\text{-}C_2B_9H_{11})_2]^-$, but this residual current could provide

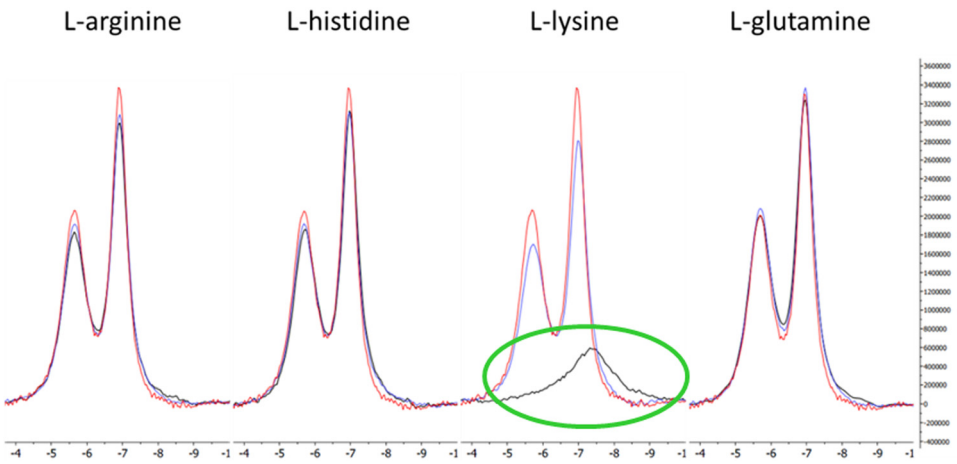

Fig. 3 $^{11}B\{^1H\}$-NMR spectra in the range of −4 to −10 ppm (B (4,4′,7,7′,9,9′,12,12′) signal region) obtained for the different mixtures of [*o*-COSAN]$^-$ and the amino acids. Na[*o*-COSAN] 2 mM as a reference appears in red, Na[*o*-COSAN] 2 mM + 2 mM of the corresponding amino acid appears in blue and Na[*o*-COSAN] 2 mM + 60 mM of the corresponding amino acid appears in black; the green circle highlights the broader signal due to interaction with L-lysine at 60 mM. The solvent used was D_2O.

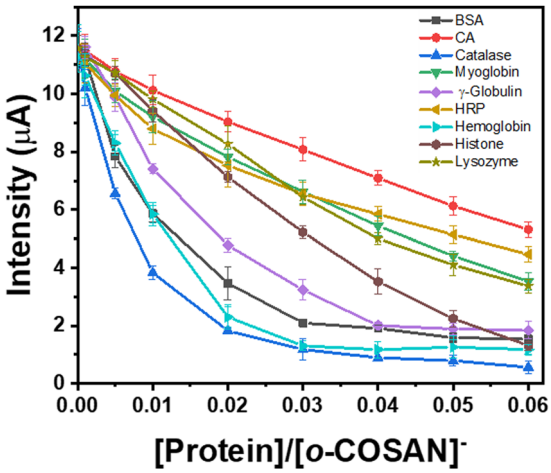

Fig. 4 The current *vs.* the ratio of protein to [*o*-COSAN]$^-$ obtained from the DPV experiment for different proteins measured in 0.1 M NaCl with glassy carbon (GC) as the working electrode and Ag/AgCl(3 M KCl) as the reference electrode.

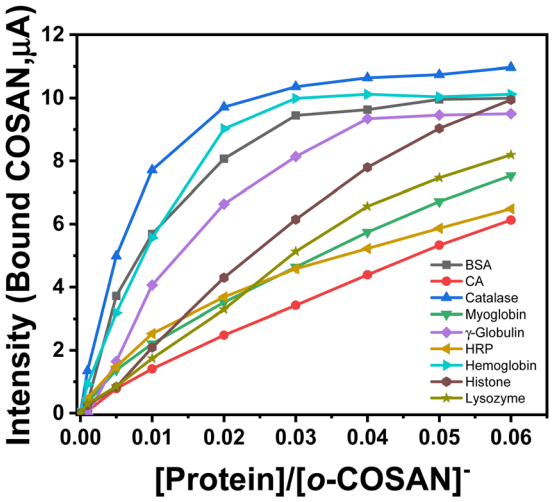

Fig. 5 The calculated intensity for the bound [*o*-COSAN]$^-$ *vs.* the protein to [*o*-COSAN]$^-$ fraction for different proteins.

deeper insights with further advancements in the technique and the development of an appropriate algorithm that would enable high-resolution visualizations of the protein surface within its natural environment. The nature of the curve is different for the different proteins indicative of an underlying factor responsible for the differences in interaction of the protein with $[3,3'\text{-Co}(1,2\text{-}C_2B_9H_{11})_2]^-$. The aim of the study is to understand and elucidate the factors responsible for these differences. For these studies, the key information is gathered from the BSA interacting with $[3,3'\text{-Co}(1,2\text{-}C_2B_9H_{11})_2]^-$, which, as mentioned earlier, can be considered ideal, as the surface obtained by DLS titration with $[3,3'\text{-Co}(1,2\text{-}C_2B_9H_{11})_2]^-$, whose dimensions are well defined, coincides with the number of basic amino residues in the protein.[38] The following plot (Fig. 4) represents the electroactive $[3,3'\text{-Co}(1,2\text{-}C_2B_9H_{11})_2]^-$ current *vs.* the [protein]/$[3,3'\text{-Co}(1,2\text{-}C_2B_9H_{11})_2]^-$ ratio at a fixed $[3,3'\text{-Co}(1,2\text{-}C_2B_9H_{11})_2]^-$ concentration of 10^{-3} M in 10^{-1} M NaCl solution (Table S1, ESI†).

Bound [*o*-COSAN]$^-$ *vs.* ratio of [protein]/[*o*-COSAN]$^-$

Since the study focuses on understanding the interaction of $[3,3'\text{-Co}(1,2\text{-}C_2B_9H_{11})_2]^-$ with the proteins, a more appropriate parameter to consider would be the amount of $[3,3'\text{-Co}(1,2\text{-}C_2B_9H_{11})_2]^-$ bound on the surface of the protein. Tentatively, we can calculate the amount of $[3,3'\text{-Co}(1,2\text{-}C_2B_9H_{11})_2]^-$ bound on the surface of a protein by taking the difference between the initial intensity of $[Co(C_2B_9H_{11})_2]^-$ in the absence of any protein and the intensity of $[3,3'\text{-Co}(1,2\text{-}C_2B_9H_{11})_2]^-$ in the presence of a protein. This is a rough estimate as some of the $[3,3'\text{-Co}(1,2\text{-}C_2B_9H_{11})_2]^-$ on the surface will be electrochemically active, but for the purpose of this research, it seems to be a fairly good approximation. Thus, if we represent bound $[Co(C_2B_9H_{11})_2]^-$ current *vs.* the [protein]/$[3,3'\text{-Co}(1,2\text{-}C_2B_9H_{11})_2]^-$ ratio, taking bound $[3,3'\text{-Co}(1,2\text{-}C_2B_9H_{11})_2]^-$ as:

Bound $[3,3'\text{-Co}(1,2\text{-}C_2B_9H_{11})_2]^-$ = Initial intensity of $[3,3'\text{-Co}(1,2\text{-}C_2B_9H_{11})_2]^-$ – Intensity of $[3,3'\text{-Co}(1,2\text{-}C_2B_9H_{11})_2]^-$ in the presence of protein, the following plot is obtained.

Fig. 5 seems to hint at two types of behaviour which we can assign as two different groups of proteins: one consisting of catalase, hemoglobin, BSA (bovine serum albumin), γ-globulin and the other having histone, HRP (horseradish peroxidase), myoglobin, lysozyme and CA (carbonic anhydrase).

Normalization of the intensity of current with respect to hydrodynamic radius (r_H)

The plots, discussed so far, only take into account the concentration but do not account for the surface area of the protein where the interactions with $[3,3'\text{-Co}(1,2\text{-}C_2B_9H_{11})_2]^-$ actually occurs. As we shall see, the currents can be roughly correlated with the surface of the proteins.

For harmonization, the factor $(r_H)^2$ has been taken into consideration, with r_H being the hydrodynamic radius of the protein. Thus, the next plot considers the normalized *current density* that is obtained by considering the $(r_H)^2$ in the denominator as:

$$\text{Normalized current density} = \text{Bound } [3,3'\text{-Co}(1,2\text{-}C_2B_9H_{11})_2]^-/(r_H)^2\ (r_H - \text{Hydrodynamic radius})$$

The hydrodynamic radius for a protein can be described as the Stokes radius, which refers to the radius of a sphere having the same hydrodynamic properties as the biomolecule.[51,52] The radii reported in these studies are obtained from the literature wherein they have been estimated in the presence of a buffer such as Tris-HCl. We have also verified these values through DLS experiments carried out in 0.1 M NaCl. In the graph, the y-axis represents the normalized *current density*, taking into consideration the surface area as r_H^2 since the surface area for a sphere is $4\pi r^2$. Table 1, Fig. 6 and Fig. S10 (ESI†) provide an overview of all the proteins studied.

Table 1 The hydrodynamic radius as well as the calculated surface area/4π, with the two different classifications of the curves as type I and type II; the two borderline proteins are highlighted in italics

Protein (Type)	Hydrodynamic radius (nm)	Surface Area/4π (nm^2)
Histone (I)	5.78	33.41
γ-Globulin (I)	5.6	31.36
Catalase (I)	5.22	27.25
BSA (I)	4.1	16.81
Hemoglobin (I)	*3.2*	*10.24*
HRP (II)	*3*	*9*
CA (II)	2.01	4.04
Lysozyme (II)	2	4
Myoglobin (II)	1.9	3.61

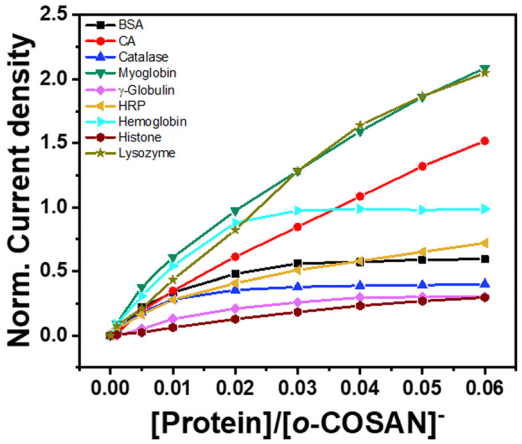

Fig. 6 The normalized current density calculated by considering the surface area of each of the protein *vs.* the protein to [*o*-COSAN]$^-$ fraction for different proteins.

After considering the surface as $(r_H)^2$, the same grouping of proteins as before is retained: γ-Globulin, catalase, BSA and hemoglobin to which the histone with some reservations could be integrated. All these proteins display a characteristic 'plateau'. With the exception of hemoglobin, all these proteins have a low maximum current density value in comparison to the remaining ones. Indeed, these proteins that exhibit a plateau attain a current density limit, while those without a plateau continue to increase, reaching values two or three times higher. Consequently, at the 0.06 [protein]/[3,3′-Co(1,2-$C_2B_9H_{11})_2]^-$ ratio, the normalized current density does not exceed 0.6 for BSA, catalase, γ-globulin, and histone, while others at this ratio show values of 1.6 for CA, 2.0 for myoglobin and lysozyme. There are two exceptions, one for each group, hemoglobin with a current density of 1.0, in the plateau group, and in the non-plateau group, HRP with 0.7.

Deductively, there are two potential types of tendencies; the former that generates a plateau (type I) and the latter having a more continuous slope (type II) as shown in Fig. 7. Consequently, two different protein/[3,3′-Co(1,2-$C_2B_9H_{11})_2]^-$ interaction models can be proposed.

The distinctive feature for each of the models proposed is their curvatures occurring at different ratios of protein/$[Co(C_2B_9H_{11})_2]^-$. Type I follows a characteristic linearity initially and eventually saturates, whereas Type II has a 'kink' initially and follows a linear path afterwards.

The proteins which follow the patterns are, as follows:

- Type I: Histone, catalase, γ-globulin, hemoglobin and BSA.
- Type II: HRP, myoglobin, lysozyme and CA.

The above behaviour models are proposed solely on the grounds of the experimental data and the following section entails plausible interpretations for the same.

Plausible explanations for the trends observed

In order to interpret the shapes of these curves on the basis of the content of basic residues in the proteins studied, and their density on the surface, we hypothesize that the basic amino acid residues are predominantly present on the protein surface owing to their hydrophilic nature and therefore, can interact strongly with [3,3′-Co(1,2-$C_2B_9H_{11})_2]^-$. Table 2 displays the number of basic amino acid residues and the total number of amino acids in the protein, which would be helpful in interpreting which other factors may be relevant in the analysis of the observed curves. Furthermore, a column has also been added to compare the number of amino acids of each protein with the protein (BSA) that has the highest number which has been assigned as 100.

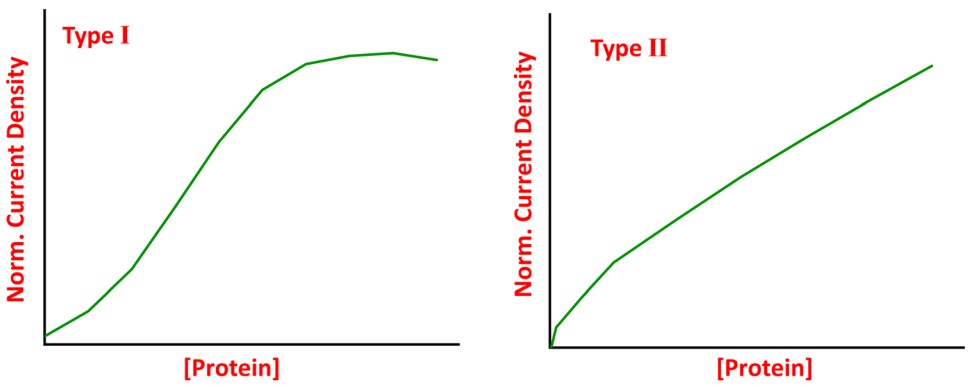

Fig. 7 Two distinctive types (I and II) of tendencies observed after normalizing the current intensity with the surface area obtained using [*o*-COSAN]$^-$ as the 'small molecule' probe.

Table 2 The different basic amino acid residues and the total number of residues present in various proteins

Protein	Lys	His	Arg	Amino acid (AA)	Norm. AA
Histone	13	5	13	133	23
Catalase	23	17	26	488	84
γ-Globulin	15	19	11	390	67
BSA	59	18	23	583	100
Hemoglobin	11	11	3	141	24
HRP	6	4	21	306	52
Myoglobin	19	13	4	151	26
Lysozyme	13	2	13	164	28
CA	24	12	7	257	44

Table 3 Calculations depicting plausible relations to the tendencies observed for the different proteins. In the 5th column, values above 1 correspond to Type I and those below 1 correspond to Type II

Protein (Type)	Basic amino acid (AA)	Basic AA/ Total AA	Basic AA/Area	(Basic AA/Total AA)*Area
Histone (I)	31	0.23	0.92	7.79
Catalase (I)	66	0.14	2.4	3.69
γ-Globulin (I)	45	0.12	1.4	3.62
BSA (I)	100	0.17	5.9	2.88
Hemoglobin (I)	25	0.18	2.4	1.82
HRP (II)	31	0.10	3.4	0.91
Myoglobin (II)	36	0.24	9.97	0.86
Lysozyme (II)	28	0.17	7	0.68
CA (II)	43	0.17	10.6	0.67

Table 3 displays the possible interpretations based on the curves observed. Based on our understanding of possible basic amino acid/$[3,3'\text{-Co}(1,2\text{-}C_2B_9H_{11})_2]^-$ interactions, we have considered the following: the number of basic amino acids, column 2; the ratio of basic amino acids to the total number of amino acids in the protein, column 3; the density of basic amino acids on the surface, column 4 and the number of basic amino acids on the surface with regard to the total number of amino acids, column 5.

In the plots described above, a saturated curve or plateau is indicative of a strong interaction between the basic residues of the protein and $[3,3'\text{-Co}(1,2\text{-}C_2B_9H_{11})_2]^-$. Typically, this is accompanied by a sharp increase in slope, indicating a strong interaction. Initially, when the concentration of $[3,3'\text{-Co}(1,2\text{-}C_2B_9H_{11})_2]^-$ exceeds that of the protein, all available binding sites in the protein will be occupied by $[3,3'\text{-Co}(1,2\text{-}C_2B_9H_{11})_2]^-$.

Considering columns 2 and 3, we observe that a dispersion of data is generated which does not correlate well with the tendencies observed. For example, if we look at column 3 (Basic AA/Total AA), there is no defined data grouping that correlates with the observed protein characteristics which may or may not lead to the formation of a plateau.

But, when we factor in the surface area, the correlation improves (column 4). Thus, for example, in column 4, three of the four proteins belonging to type II are those which have the highest density of basic amino acids. HRP is the discordant figure among this set of non-plateau-forming proteins, contrasting with BSA in the other group. But this correlation improves dramatically when we consider the number of basic amino acids on the surface with regard to the total number of amino acids. In this case, there is a perfect correlation. The two groups of data generated agree well with the two experimental groups, the former that generates a plateau and the latter which doesn't. Conceptually, the density of amino acids and the total number of amino acids in a protein with certain dimensions are related, but the most relevant difference is that of considering how many basic amino acids exist with respect to the total, which indirectly considers the non-basic characteristics of the other amino acids within the protein.

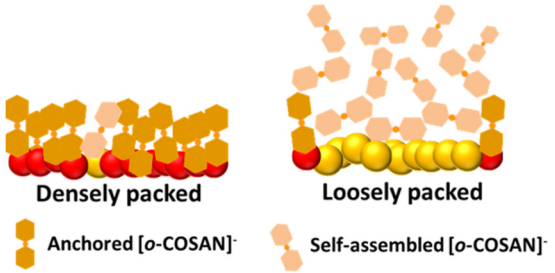

Fig. 8 A visual representation of the two types of protein-[o-COSAN]$^-$ interactions observed with regard to the two groups of classification obtained, where the basic amino acid residues are represented in red and the other amino acid residues in yellow.

The reason why one group of proteins has a curve with a marked limit of $[3,3'\text{-Co}(1,2\text{-}C_2B_9H_{11})_2]^-$ and the other does not is yet to be determined. The explanation is sustained by the fact that in the former, there is a higher proportion of basic amino acids compared to the total, allowing a greater number of $[3,3'\text{-Co}(1,2\text{-}C_2B_9H_{11})_2]^-$ molecules to interact in an end-on disposition, thus forming a robust coating with well-ordered $[3,3'\text{-Co}(1,2\text{-}C_2B_9H_{11})_2]^-$, preventing further growth by self-assembling of $[3,3'\text{-Co}(1,2\text{-}C_2B_9H_{11})_2]^-$ (Fig. 8). On the other end are proteins having a smaller ratio of basic amino acids which are surrounded by non-basic amino acids that do not interact with the $[3,3'\text{-Co}(C_2B_9H_{11})_2]^-$ molecules. In this scenario, only $[3,3'\text{-Co}(1,2\text{-}C_2B_9H_{11})_2]^-$ interacting with the basic residues adopts an end-on orientation. If the basic residues are in close proximity, the end-on alignment is preserved; the latter orientation can expand outward, accounting for the continued growth of $[3,3'\text{-Co}(1,2\text{-}C_2B_9H_{11})_2]^-$. By meticulously analysing the current profile relative to protein concentration using an appropriate algorithm, it becomes possible to obtain a high-resolution depiction of the surface in its natural environment. Thus, two sets of $[3,3'\text{-Co}(1,2\text{-}C_2B_9H_{11})_2]^-$ can be postulated to be on the surface, those that are ordered due to their interaction with the basic residue and those that are not. These loosely packed $[3,3'\text{-Co}(1,2\text{-}C_2B_9H_{11})_2]^-$ facilitates self-assembly which allows unlimited growth in the number of $[3,3'\text{-Co}(1,2\text{-}C_2B_9H_{11})_2]^-$ and thereby extending the dimension of the protein/$[3,3'\text{-Co}(1,2\text{-}C_2B_9H_{11})_2]^-$ assembly (Fig. 8). Therefore, the proteins could be classified as High Surface Base Density

(HSBD) (Type I) and Low Surface Base Density (LSBD) (Type II), which can be distinguished using [*o*-COSAN]$^-$ as an electrochemical molecular probe.

Indeed, these models are consistent with the higher current intensity for the type II proteins *vs.* type I. Notably, it can be observed that the intensity related to bound [3,3′-Co(1,2-$C_2B_9H_{11})_2$]$^-$ can reach up to 50% in some type II molecules (Fig. 4), indicating that the bonded [3,3′-Co(1,2-$C_2B_9H_{11})_2$]$^-$ molecules have more relaxed binding, enabling better interaction with the electrode through exchange phenomena. A further insight into the relevance of the surface represented by $(r_H)^2$ is obtained if the focus is set on the hydrodynamic radius and a graph of the normalised intensity is plotted against the hydrodynamic radius, each at different protein fractions, 0.03, 0.04, 0.05 and 0.06 as shown in Fig. 9 (Fig. S11, ESI†). At the lower protein fractions, a linear relation is obtained. These changes result in a non-linear relation at the two higher protein fractions. However, all of them provide the same information as seen in the following plots. The information is complementary to the former interpretation of the earlier plots and basically *indicates that size and surface behaviour are related*.

In each of the plots (Fig. 9), it can be observed that as the hydrodynamic radius increases, the amount of [3,3′-Co(1,2-$C_2B_9H_{11})_2$]$^-$ bound on the surface of the protein decreases. A smaller radius implies a higher surface to volume ratio. Hence, it can be assumed that the density of the amino acids, particularly the polar ones, is higher on the surface for smaller proteins as compared to larger ones. As a result, the amino acids which act as an anchoring point for [3,3′-Co(1,2-$C_2B_9H_{11})_2$]$^-$ would be in close proximity of one another and result in a more densely packed structure. Consequently, the amount of [3,3′-Co(1,2-$C_2B_9H_{11})_2$]$^-$ bound on the protein surface would be higher. This would imply that smaller the protein, higher would be [3,3′-Co(1,2-$C_2B_9H_{11})_2$]$^-$ density on the surface.

As can be observed from the graphs, LSBD proteins (CA and HRP) tend to deviate from the trendline but seem to be in order with each other. The deviation can be accounted by considering the fact that the surface area obtained from the hydrodynamic radius may vary from the 'effective' protein surface owing to the different protein structures. The more the difference from the 'effective' surface, more would be the deviation from the trendline. Hence, it is rational to consider that for proteins such as CA and HRP, the deviation from the 'effective' surface is much more prominent than the others. In some ways, this deviation and its magnitude indicate how the defect-free spherical surface is altered by the existence of voids and/or moors, depicting a more realistic view of the interacting surface of a protein.

Influence of the electrolyte

The electrochemical measurements in this study were performed in the presence of an electrolyte, NaCl, in order for the electroactive substance to access the electrode through a

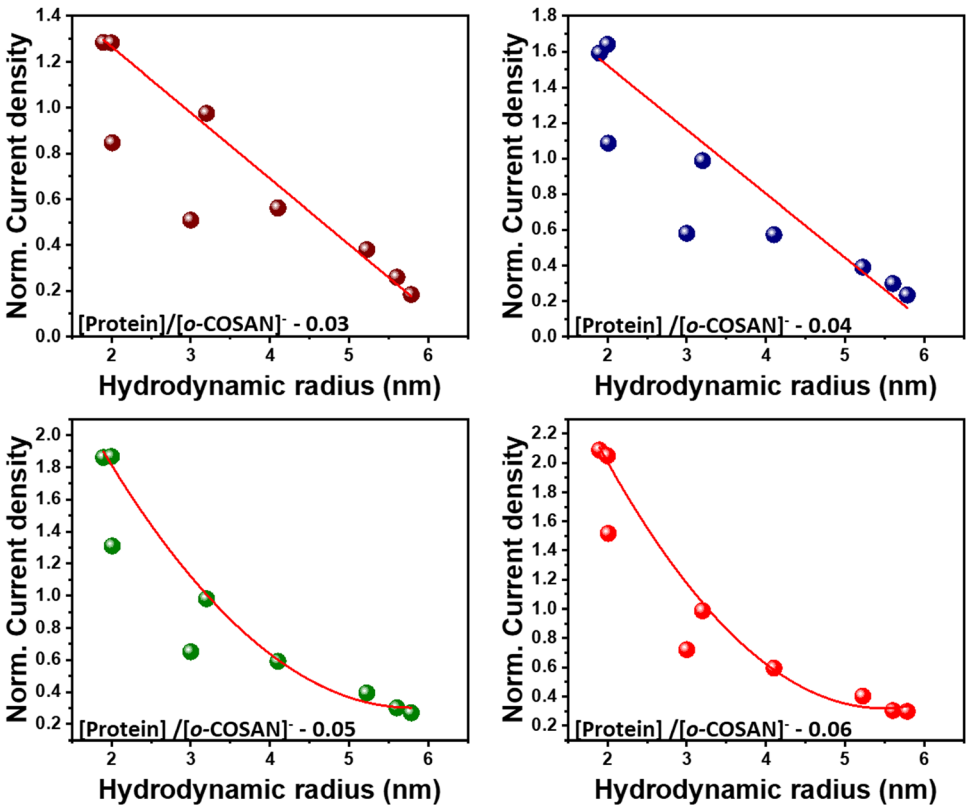

Fig. 9 The normalized current density *vs.* the hydrodynamic radius at different protein/[*o*-COSAN]$^-$ ratios from 0.03 to 0.06. [From smallest to largest hydrodynamic radius: Myoglobin, lysozyme, CA, HRP, hemoglobin, BSA, catalase, γ-globulin and histone].

Table 4 The number of [*o*-COSAN]$^-$ present on the HSBD protein surface

Protein	Hydrodynamic radius (nm)	Intersection (point of maximum coverage)	Number of [*o*-COSAN]$^-$ (experimental)
Histone	5.78	0.041	25
γ-Globulin	5.6	0.027	37
Catalase	5.2	0.013	77
BSA	4.1	0.012	83
Hemoglobin	3.2	0.020	50

diffusion process. In such a scenario where two anions are present, namely Cl^- and $[3,3'\text{-}Co(1,2\text{-}C_2B_9H_{11})_2]^-$ in the ratio 100 : 1, there's a possible competition between the two to occupy the protein surface. In the case of the Cl^- ion, the primary interaction that would come into play would be electrostatics, whereas for $[3,3'\text{-}Co(1,2\text{-}C_2B_9H_{11})_2]^-$, it would involve both electrostatic interaction as well as the N–H···H–B dihydrogen bonds.[41] For these reasons, the interaction of $[3,3'\text{-}Co(1,2\text{-}C_2B_9H_{11})_2]^-$ with the protein is stronger as it is able to displace Cl^- despite the electrolyte being at high concentration in comparison to $[3,3'\text{-}Co(1,2\text{-}C_2B_9H_{11})_2]^-$. Another interesting point to reflect on in such studies is the radius of the proteins. The radii used to account for the surface area of the proteins are the hydrodynamic radii measured under specific conditions. The hydrodynamic radius is mainly representative of the ideal flawless protein surface rather than the reactive functional one with its voids and moors. In this work, DLS measurements were performed in NaCl and the hydrodynamic radii of the different proteins confer with the reported values in buffer solutions (Fig. S12 and Table S2, ESI†). In a previous work, we had studied the interaction of $[3,3'\text{-}Co(1,2\text{-}C_2B_9H_{11})_2]^-$ and BSA in the absence of any electrolyte, only water, and found that the hydrodynamic radius of BSA was 1.6 nm which is smaller in comparison to 4.1 nm reported in this study. This in itself proves the importance and influence of anions and their co-ions in determining the diameter of the protein. If we consider the High Surface Base Density (HSBD) (Type I) proteins such as BSA, catalase, γ-globulin, hemoglobin and histone, an intersecting point corresponding to a particular [protein]/$[3,3'\text{-}Co(1,2\text{-}C_2B_9H_{11})_2]^-$ value can be observed. This point is highly significant as this is the maximum number of tightly bound $[3,3'\text{-}Co(1,2\text{-}C_2B_9H_{11})_2]^-$ molecules that can be present on a single protein molecule. Thus, this is a key number to get an estimate of the number of $[3,3'\text{-}Co(1,2\text{-}C_2B_9H_{11})_2]^-$ molecules on the protein's surface. As can be seen in Table 4, as the protein size increases, the amount of $[3,3'\text{-}Co(1,2\text{-}C_2B_9H_{11})_2]^-$ present on the surface decreases. Hemoglobin is an exception to this general rule, but that can be attributed to the fact that it is on the borderline between HSBD (type I) and Low Surface Base Density (LSBD) (Type II) proteins, as shown in Table 3.

Interestingly, the number of $[3,3'\text{-}Co(1,2\text{-}C_2B_9H_{11})_2]^-$ on the BSA surface is lower in comparison to the study performed in the absence of any electrolyte which was calculated to be 100.[38] What caused this? The answer would simply be the environment in which the protein is surrounded which greatly defines the surface area available. Forthwith, we could state that the water molecules are much more labile and easily replaceable compared to the anions and co-ions of the surroundings that are at a much higher concentration than the $[3,3'\text{-}Co(1,2\text{-}C_2B_9H_{11})_2]^-$ molecules. Secondly, the existing anions and co-ions, as they are not so easily displaced, are retained and form a relatively persistent layer on which the $[3,3'\text{-}Co(1,2\text{-}C_2B_9H_{11})_2]^-$ molecules are deposited which would interfere with the interaction of $[3,3'\text{-}Co(1,2\text{-}C_2B_9H_{11})_2]^-$ with the protein surface. A competition would exist that would depend on the concentration of the competing ions and their relative affinity for the basic residues. Despite all these simplifications used, the results generally seem to be realistic enough to be useful.

Conclusion

This study proves the complexity of what we consider as the 'surface' of a protein. In this study, we have attempted to address the 'surface' of a protein considering the 'effective' protein surface (EPS) with regard to its interaction with the 'small molecule' probe, $[3,3'\text{-}Co(1,2\text{-}C_2B_9H_{11})_2]^-$. We were able to use simple and rational estimations and calculations to explain the tendencies observed in terms of the $[3,3'\text{-}Co(1,2\text{-}C_2B_9H_{11})_2]^-$/protein interactions. We had deliberately used a small molecule that is anionic, redox-active, capable of self-assembly and of producing hydrogen and dihydrogen non-bonding interactions to demonstrate the potential of small molecules with unique characteristics as 'molecular probes' for better visualizations. We were able to demonstrate the correlation of size and polar amino acid residues to the interactions with $[3,3'\text{-}Co(1,2\text{-}C_2B_9H_{11})_2]^-$. We have also shown how the environment of the protein affects the interactions as well as tunes the self-assembly of $[3,3'\text{-}Co(1,2\text{-}C_2B_9H_{11})_2]^-$ and therefore affects the measurements involved. We were indeed, able to demonstrate that $[3,3'\text{-}Co(1,2\text{-}C_2B_9H_{11})_2]^-$ 'viewed' each protein surface differently and hence has the potential to act as a simple and easy to handle cantilever for measuring and picturing the protein surfaces. We have described a novel method for the analysis of a protein in its intrinsic form and environment without any interference. With this work, we aimed to open an avenue for extended research in understanding the surface of a protein particularly using small unique molecular probes such as $[3,3'\text{-}Co(1,2\text{-}C_2B_9H_{11})_2]^-$. Although these comparisons have been carried out experimentally, we are certain that employing a suitable algorithm would allow for high-resolution visualizations of the protein surface in its natural environment.

Author contributions

Conceptualization, F. T. and C. V.; methodology, F. T., J. A. M. X., I. F. and M. N.-M.; formal analysis, F. T., C. V., J. A. and M. X.; writing—original draft preparation, F. T., J. A. M. X. and C. V.; writing—review and editing, all the authors.

Conflicts of interest

The authors declare no conflicts of interest.

Acknowledgements

This work received funding from the Spanish Ministry of Science, through the ''Severo Ochoa'' Programme for Centres of Excellence in R&D (CEX2019-000917-S) as well as the Spanish Ministerio de Ciencia e Innovación (PID2019-106832RB-I00) and Generalitat de Catalunya (2017SGR1720). J. A. M. Xavier acknowledges the DOC-FAM programme under the Marie Sklodowska-Curie grant agreement No. 754397 and is enrolled in the PhD programme in UAB.

References

1 C. I. Branden and J. Tooze, *Introduction to Protein Structure*, Garland Science, 2nd edn, 2012.
2 C. A. Orengo, A. E. Todd and J. M. Thornton, From protein structure to function, *Curr. Opin. Struct. Biol.*, 1999, **9**, 374–382.
3 G. N. Ramachandran, C. Ramakrishnan and V. Sasisekharan, Stereochemistry of polypeptide chain configurations, *J. Mol. Biol.*, 1963, **7**, 95–99.
4 R. M. Jackson and M. J. E. Sternberg, Protein surface area defined, *Nature*, 1993, **366**, 638.
5 V. N. Uversky, Intrinsically disordered proteins from A to Z, *Int. J. Biochem. Cell Biol.*, 2011, **43**, 1090–1103.
6 C. J. Oldfield, Y. Cheng, M. S. Cortese, C. J. Brown, V. N. Uversky and A. K. Dunker, Comparing and Combining Predictors of Mostly Disordered Proteins, *Biochemistry*, 2005, **44**, 1989–2000.
7 K. Mazmanian, K. Sargsyan and C. Lim, How the Local Environment of Functional Sites Regulates Protein Function, *J. Am. Chem. Soc.*, 2020, **142**, 9861–9871.
8 S. L. Speer, W. Zheng, X. Jiang, I.-T. Chu, A. J. Guseman, M. Liu, G. J. Pielak and C. Li, The intracellular environment affects protein–protein interactions, *Proc. Natl. Acad. Sci. U. S. A.*, 2021, **118**(11), e2019918118.
9 B. Yu, C. C. Pletka and J. Iwahara, Quantifying and visualizing weak interactions between anions and proteins, *Proc. Natl. Acad. Sci. U. S. A.*, 2021, **118**(2), e2015879118.
10 Y. Okuno, J. Yoo, C. D. Schwieters, R. B. Best, H. S. Chung and G. M. Clore, Atomic view of cosolute-induced protein denaturation probed by NMR solvent paramagnetic relaxation enhancement, *Proc. Natl. Acad. Sci. U. S. A.*, 2021, **118**(34), e2112021118.
11 Z. Jing, R. Qi, C. Liu and P. Ren, Study of interactions between metal ions and protein model compounds by energy decomposition analyses and the AMOEBA force field, *J. Chem. Phys.*, 2017, **147**, 161733.
12 M. Ozboyaci, D. B. Kokh, S. Corni and R. C. Wade, Modeling and simulation of protein-surface interactions: achievements and challenges, *Q. Rev. Biophys.*, 2016, **49**, e4.
13 T. C. Terwilliger, D. Stuart and S. Yokoyama, Lessons from Structural Genomics, *Annu. Rev. Biophys.*, 2009, **38**, 371–383.
14 C. J. Lanci, C. M. MacDermaid, S. Kang, R. Acharya, B. North, X. Yang, X. J. Qiu, W. F. DeGrado and J. G. Saven, Computational design of a protein crystal, *Proc. Natl. Acad. Sci. U. S. A.*, 2012, **109**, 7304–7309.
15 E. Laine and A. Carbone, Local Geometry and Evolutionary Conservation of Protein Surfaces Reveal the Multiple Recognition Patches in Protein-Protein Interactions, *PLoS Comput. Biol.*, 2015, **11**, 1–32.
16 L. Ronda, S. Bruno, S. Bettati, P. Storici and A. Mozzarelli, From protein structure to function via single crystal optical spectroscopy, *Front. Mol. Biosci.*, 2015, **2**, 2296.
17 U. Heinemann, K. Büssow, U. Mueller and P. Umbach, Facilities and Methods for the High-Throughput Crystal Structural Analysis of Human Proteins, *Acc. Chem. Res.*, 2003, **36**, 157–163.
18 K. Palczewski, T. Kumasaka, T. Hori, C. A. Behnke, H. Motoshima, B. A. Fox, I. Le Trong, D. C. Teller, T. Okada, R. E. Stenkamp, M. Yamamoto and M. Miyano, Crystal Structure of Rhodopsin: A G Protein-Coupled Receptor, *Science*, 2000, **289**, 739–745.
19 Y. Hu, K. Cheng, L. He, X. Zhang, B. Jiang, L. Jiang, C. Li, G. Wang, Y. Yang and M. Liu, NMR-Based Methods for Protein Analysis, *Anal. Chem.*, 2021, **93**, 1866–1879.
20 K. Murata and M. Wolf, Cryo-electron microscopy for structural analysis of dynamic biological macromolecules, *Biochim. Biophys. Acta, Gen. Subj.*, 2018, **1862**, 324–334.
21 Y. Yue, T. Zhao, Y. Wang, K. Ma, X. Wu, F. Huo, F. Cheng and C. Yin, HSA-Lys-161 covalent bound fluorescent dye for in vivo blood drug dynamic imaging and tumor mapping, *Chem. Sci.*, 2022, **13**, 218–224.
22 Y. Yue, T. Zhao, Z. Xu, W. Chi, X. Chai, J. Ai, J. Zhang, F. Huo, R. M. Strongin and C. Yin, Enlarging the Stokes Shift by Weakening the π-Conjugation of Cyanines for High Signal-to-Noise Ratiometric Imaging, *Adv. Sci.*, 2023, **10**, 2205080.
23 F. Zhao, S. M. Matt, J. Bu, O. G. Rehrauer, D. Ben-Amotz and S. A. McLuckey, Joule Heating and Thermal Denaturation of Proteins in Nano-ESI Theta Tips, *J. Am. Soc. Mass Spectrom.*, 2017, **28**, 2001–2010.
24 K. J. Freedman, S. R. Haq, J. B. Edel, P. Jemth and M. J. Kim, Single molecule unfolding and stretching of protein domains inside a solid-state nanopore by electric field, *Sci. Rep.*, 2013, **3**, 1638.
25 W. Chen, Electroconformational denaturation of membrane proteins, *Ann. N. Y. Acad. Sci.*, 2005, **1066**, 92–105.

26 E. V. Suprun, Direct electrochemistry of proteins and nucleic acids: The focus on 3D structure, *Electrochem. Commun.*, 2021, **125**, 106983.
27 M. Uchman, V. Ďorďovič, Z. Tošner and P. Matějíček, Classical Amphiphilic Behavior of Nonclassical Amphiphiles: A Comparison of Metallacarborane Self-Assembly with SDS Micellization, *Angew. Chem.*, 2015, **54**, 14113–14117.
28 D. C. Malaspina, C. Viñas, F. Teixidor and J. Faraudo, Atomistic Simulations of COSAN: Amphiphiles without a Head-and-Tail Design Display ''Head and Tail'' Surfactant Behavior, *Angew. Chem.*, 2020, **59**, 3088–3092.
29 P. Bauduin, S. Prevost, P. Farràs, F. Teixidor, O. Diat and T. Zemb, A Theta-Shaped Amphiphilic Cobaltabisdicarbollide Anion: Transition From Monolayer Vesicles to Micelles, *Angew. Chem.*, 2011, **50**, 5298–5300.
30 P. Farràs, E. J. Juárez-Pérez, M. Lepšík, R. Luque, R. Núñez and F. Teixidor, Metallacarboranes and their interactions: theoretical insights and their applicability, *Chem. Soc. Rev.*, 2012, **41**, 3445–3463.
31 R. N. Grimes, *Carboranes*, Elsevier Inc, New York, 3rd edn, 2016.
32 M. Tarrés, C. Viñas, A. M. Cioran, M. M. Hänninen, R. Sillanpää and F. Teixidor, Towards Multifunctional Materials Incorporating Elastomers and Reversible Redox-Active Fragments, *Chem. – Eur. J.*, 2014, **20**, 15808–15815.
33 D. Tu, H. Yan, J. Poater and M. Solà, The *nido*-Cage···π Bond: A Non-covalent Interaction between Boron Clusters and Aromatic Rings and Its Applications, *Angew. Chem.*, 2020, **59**, 9018–9025.
34 C. Viñas, M. Tarrés, P. González-Cardoso, P. Farràs, P. Bauduin and F. Teixidor, Surfactant behaviour of metallacarboranes. A study based on the electrolysis of water, *Dalton Trans.*, 2014, **43**, 5062–5068.
35 J. A. M. Xavier, C. Viñas, E. Lorenzo, T. García-Mendiola and F. Teixidor, Potential application of metallacarboranes as an internal reference: an electrochemical comparative study to ferrocene, *Chem. Commun.*, 2022, **58**, 4196–4199.
36 J.-N. Longchamp, S. Rauschenbach, S. Abb, C. Escher, T. Latychevskaia, K. Kern and H.-W. Fink, Imaging proteins at the single-molecule level, *Proc. Natl. Acad. Sci. U. S. A.*, 2017, **114**, 1474–1479.
37 T. O. Pleshakova, N. S. Bukharina, A. I. Archakov and Y. D. Ivanov, Atomic Force Microscopy for Protein Detection and Their Physicochemical Characterization, *Int. J. Mol. Sci.*, 2018, **19**, 1142.
38 I. Fuentes, J. Pujols, C. Viñas, S. Ventura and F. Teixidor, Dual Binding Mode of Metallacarborane Produces a Robust Shield on Proteins, *Chemistry*, 2019, **25**, 12820–12829.
39 M. Y. Losytskyy, V. B. Kovalska, O. A. Varzatskii, M. V. Kuperman, S. Potocki, E. Gumienna-Kontecka, A. P. Zhdanov, S. M. Yarmoluk, Y. Z. Voloshin, K. Y. Zhizhin, N. T. Kuznetsov and A. V. Elskaya, An interaction of the functionalized closo-borates with albumins: The protein fluorescence quenching and calorimetry study, *J. Lumin.*, 2016, **169**, 51–60.
40 T. M. Goszczyński, K. Fink, K. Kowalski, Z. J. Leśnikowski and J. Boratyński, Interactions of Boron Clusters and their Derivatives with Serum Albumin, *Sci. Rep.*, 2017, **7**, 9800.
41 A.-I. Stoica, C. Kleber, C. Viñas and F. Teixidor, Ion selective electrodes for protonable nitrogen containing analytes: Metallacarboranes as active membrane components, *Electrochim. Acta*, 2013, **113**, 94–98.
42 A.-I. Stoica, C. Viñas and F. Teixidor, Cobaltabisdicarbollide anion receptor for enantiomer-selective membrane electrodes, *Chem. Commun.*, 2009, 4988–4990.
43 K. Fink, J. Boratyński, M. Paprocka and T. M. Goszczyński, Metallacarboranes as a tool for enhancing the activity of therapeutic peptides, *Ann. New York Acad. Sci.*, 2019, **1457**, 128–141.
44 M.-C. Bellissent-Funel, A. Hassanali, M. Havenith, R. Henchman, P. Pohl, F. Sterpone, D. van der Spoel, Y. Xu and A. E. Garcia, Water Determines the Structure and Dynamics of Proteins, *Chem. Rev.*, 2016, **116**, 7673–7697.
45 R. Núñez, M. Tarrés, A. Ferrer-Ugalde, F. F. De Biani and F. Teixidor, Electrochemistry and Photoluminescence of Icosahedral Carboranes, Boranes, Metallacarboranes, and Their Derivatives, *Chem. Rev.*, 2016, **116**, 14307–14378.
46 H. I. Okur, J. Hladílková, K. B. Rembert, Y. Cho, J. Heyda, J. Dzubiella, P. S. Cremer and P. Jungwirth, Beyond the Hofmeister Series: Ion-Specific Effects on Proteins and Their Biological Functions, *J. Phys. Chem. B*, 2017, **121**, 1997–2014.
47 M. G. Cacace, E. M. Landau and J. J. Ramsden, The Hofmeister series: salt and solvent effects on interfacial phenomena, *Q. Rev. Biophys.*, 1997, **30**, 241–277.
48 A.-I. Stoica, C. Viñas and F. Teixidor, History of Cobaltabis(dicarbollide) in Potentiometry, No Need for Ionophores to Get an Excellent Selectivity, *Molecules*, 2022, **27**, 8312.
49 I. Guerrero, A. Saha, J. A. M. Xavier, C. Viñas, I. Romero and F. Teixidor, Noncovalently Linked Metallacarboranes on Functionalized Magnetic Nanoparticles as Highly Efficient, Robust, and Reusable Photocatalysts in Aqueous Medium, *ACS Appl. Mater. Interfaces*, 2020, **12**, 56372–56384.
50 T. García-Mendiola, V. Bayon-Pizarro, A. Zaulet, I. Fuentes, F. Pariente, F. Teixidor, C. Viñas and E. Lorenzo, Metallacarboranes as tunable redox potential electrochemical indicators for screening of gene mutation, *Chem. Sci.*, 2016, **7**, 5786–5797.
51 H. P. Erickson, Size and shape of protein molecules at the nanometer level determined by sedimentation, gel filtration, and electron microscopy, *Biol. Proced. Online*, 2009, **11**, 32–51.
52 V. La Verde, P. Dominici and A. Astegno, Determination of Hydrodynamic Radius of Proteins by Size Exclusion Chromatography, *Bio-protocol*, 2017, **7**, e2230.

